

# Enhancing Visible-Light Photocatalysis *via* Endohedral Functionalization of Single-Walled Carbon Nanotubes with Organic Dyes

Daniel González-Muñoz, Ana Martín-Somer, Klara Strobl, Silvia Cabrera, Pedro J. De Pablo, Sergio Díaz-Tendero, Matías Blanco,\* and José Alemán\*



Cite This: *ACS Appl. Mater. Interfaces* 2021, 13, 24877–24886



Read Online

ACCESS |



Metrics & More



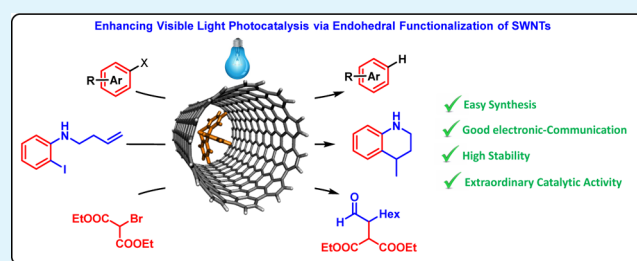
Article Recommendations



Supporting Information

**ABSTRACT:** The encapsulation of an organic dye, 10-phenylphenothiazine (PTH), in the inner cavity of single-walled carbon nanotubes (SWNTs) as a breaking heterogenization strategy is presented. The PTH@oSWNT material was microscopically and spectroscopically characterized, showing intense photoemission when illuminated with visible light at the nanoscale. Thus, PTH@oSWNT was employed as a heterogeneous photocatalyst in single electron transfer dehalogenation reactions under visible light irradiation. The material showed an enhanced photocatalytic activity, achieving turnover numbers as high as 3200, with complete recyclability and stability for more than eight cycles. Computational calculations confirm that electronic communication between both partners is established because, upon illumination, an electron of the excited PTH is transferred from the  $\pi$  system of the molecule to the delocalized  $\pi$ -cloud of the SWNT, thus justifying the enhanced photocatalytic activity.

**KEYWORDS:** photocatalysis, nanotubes, materials, computational calculations, visible light



## 1. INTRODUCTION

Single-walled carbon nanotubes (SWNTs) are unique allotropes of carbon which are classified as 1D materials<sup>1,2</sup> with astonishing properties.<sup>2–4</sup> Chemical reactions catalyzed by bare SWNTs are still very narrow,<sup>5,6</sup> and functionalization treatments<sup>7–9</sup> are routinely performed to enlarge their potential application in chemical catalysis, electrocatalysis, and also photocatalysis. In this regard, several examples have been reported where SWNTs form the conductive partner of nanocomposites, which are typically combined with inorganic photosensitizers, such as TiO<sub>2</sub><sup>10,11</sup> and ZnS<sup>12</sup> among others,<sup>13–17</sup> usually under UV light conditions. By contrast, visible-light photocatalysis in organic synthesis has appeared as an alternative to UV irradiation and as a new powerful tool for achieving novel chemical transformations,<sup>14–17</sup> obtaining, in many cases, radicals *via* single electron transfer reactions (SETs)<sup>18</sup> or energy-transfer processes.<sup>19</sup> Thus, it has enabled a change from previous protocols based on toxic reagents and harsh reaction conditions. In this field, two types of homogeneous photocatalysts have appeared: transition metals, which are usually very stable but extremely expensive (*e.g.*, Ir, Ru, and Pt),<sup>20</sup> and organic dyes,<sup>15</sup> which, although cheap, are not robust under photocatalytic conditions. Therefore, it would be desirable to find new strategies for protecting the organic photocatalyst with a good catalytic performance and greater applicability and durability. In addition, the homo-

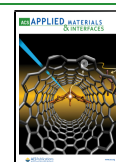
geneous photocatalyst recovery is tedious and usually prevents its recyclability.

Two main strategies have been used to functionalize SWNTs with visible-light photocatalysts.<sup>7,8</sup> The first consists of the physisorption of the photocatalyst at the nanotube surface, which is a fast and easy strategy without the need for synthetic modifications of the photocatalyst and the nanotube (Scheme 1A). An adequate geometry amid both structures is necessary for an optimal interaction, and generally a good electronic communication is obtained that yields good photocatalytic results.<sup>21</sup> However, the stability of the resulting hybrid material is often low, given the weak interaction of physisorption, and therefore, the durability and recyclability are compromised under photocatalytic conditions.<sup>22,23</sup> Alternatively, the nanotube and the photocatalyst can be covalently bonded, allowing better recyclability and durability (Scheme 1B).<sup>24</sup> However, this procedure entails a greater synthetic effort since a deep photocatalyst modification, a suitable binding protocol (usually through the amide bond formation,

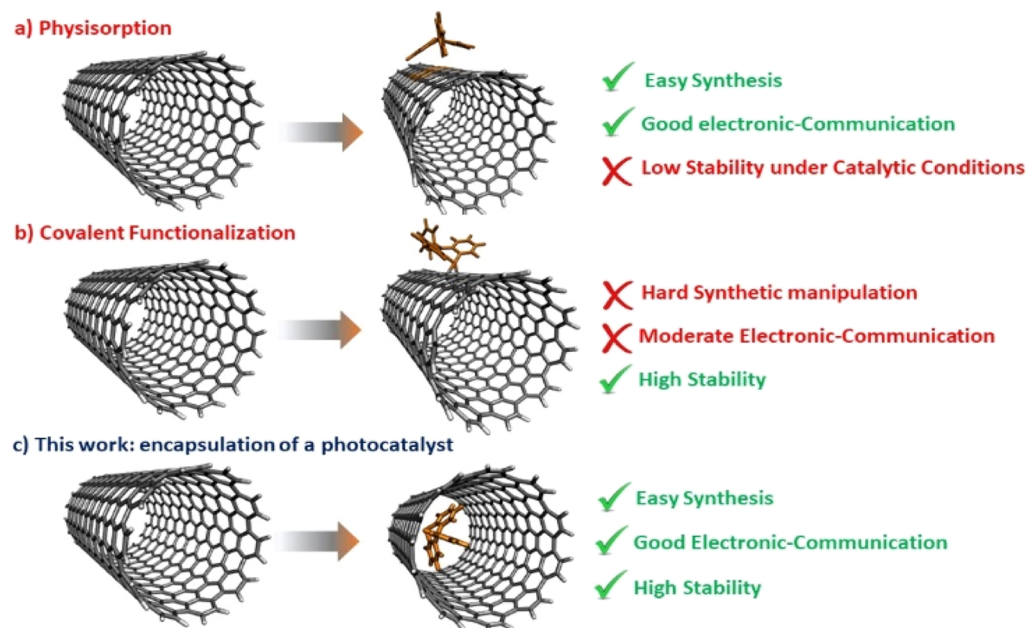
Received: March 12, 2021

Accepted: April 20, 2021

Published: May 7, 2021



Scheme 1. Different Strategies in Photocatalyst Nanotube Hybrid Materials for Organic Synthesis: (a) Physisorption, (b) Covalent Attachment, and in This Work, (c) Photocatalyst Encapsulated in the Nanotube



diazonium radical addition, *etc.*), and additional synthetic modifications at the nanotube surface are needed. Additionally, the geometry imposed by the covalent bond between the photocatalyst and the carbon nanomaterial may, on occasions, result in inefficient electronic communication among both partners, which turns the nanotube into a mere heterogeneous support to carry out the photochemical reaction without any synergistic effect. Interestingly, some reports have shown the possibility of introducing molecules at the inner cavity of the nanotube, the so-called endohedral functionalization.<sup>25</sup> The encapsulation strategy presents the advantages of noncovalent functionalization of the nanotubes, which preserves the structure and therefore the properties of pristine SWNTs, with outstanding stability toward reaction conditions that the covalent functionalization provides.<sup>26,27</sup> To the best of our knowledge, the encapsulation of organic photocatalysts has never been applied for photocatalytic reactions in organic synthesis (Scheme 1C).

Therefore, in this work, we propose a new photocatalytic strategy, which consists of the introduction of a photocatalyst inside the nanotube structure, avoiding the synthetic modifications of the photocatalyst and the SWNTs. It is expected that the encapsulation of the photocatalyst within the inner cavity of the SWNT will afford a better catalytic performance due to the protection that the nanotube provides to the organic photocatalyst under the photocatalytic conditions. Moreover, the combination of experimental proofs and density functional theory (DFT) calculations enables us to understand the mechanism behind the synergistic effect caused by the photocatalyst and the SWNT.

## 2. EXPERIMENTAL SECTION

**2.1. Synthesis of Phenylphenothiazine Photocatalyst.** 10-Phenylphenothiazine (PTH, **1**) was synthesized according to previous reports (see Supporting Information for further details). Spectroscopic data are in agreement with the published data.

**2.2. Nanotubes Cap Opening: Synthesis of oSWNT (3).** In a typical experiment, 50 mg of pristine and closed SWNTs [cSWNT

(2) sample] was added in an open flask with 50 mL of concentrated hydrochloric acid, and the mixture was magnetically stirred at 60 °C for 2 h. After cooling down, the solid was isolated by centrifugation and washed with fresh Milli-Q water with the necessary centrifugation cycles till the supernatant reached neutral pH. After drying under vacuum, the procedure yielded the sample oSWNT (3).

**2.3. PTH Encapsulation: Synthesis of PTH@oSWNT (5).** In a typical experiment, 70 mg of PTH and 7 mg of oSWNT were suspended under nitrogen atmosphere in 3.5 mL of *N,N*-dimethylformamide (DMF), and the mixture was magnetically stirred at reflux conditions for 16 h. Then, the mixture was allowed to cool down naturally, and the suspension was filtered through a 0.45  $\mu$ m polypropylene (PP) membrane. The black powder was collected, suspended in 20 mL of fresh DMF with the help of 5 min of sonication, and filtered again. This washing procedure was repeated three additional times with DMF, three cycles with dichloromethane (DCM), and three cycles with acetone. Drying under vacuum yielded the sample PTH@oSWNT (5).

**2.4. Synthesis of PTH·cSWNT (4).** This material was prepared by contacting for 15 min a determined amount of a 0.01 M acetonitrile solution of PTH (0.08 mg,  $2.91 \times 10^{-4}$  mmol) with 1 mg of cSWNT to fulfill the 8% wt without washing the sample for not removing the physisorbed molecule. After drying under vacuum, the procedure yielded the sample PTH·cSWNT (4). In addition, a control sample (4') was prepared by refluxing 1 mg of cSWNT in the presence of the same 0.01 M acetonitrile solution of PTH (0.08 mg,  $2.91 \times 10^{-4}$  mmol) following a protocol identical to that of sample 4.

**2.5. General Procedure for Photocatalytic Debromination.** A vial was charged with a magnetic stirring bar, the halogenated substrate **6a–r** (0.1 mmol), the catalyst [1 mg for nanotubes-based materials, 0.29 or 5 mol % for PTH (**1**)], CH<sub>3</sub>CN (1 mL), HCOOH (0.5 mmol), and Bu<sub>3</sub>N (0.5 mmol). The vial was sealed and degassed by three freeze–pump–thaw cycles. The blue LEDs of the reactor were turned on, and the reaction was allowed to proceed at room temperature for the desired time, typically 16 h. A 0.05–0.1 mL aliquot was withdrawn at regular intervals and analyzed by NMR spectroscopy to monitor the progress of the reaction. Yields of volatile products were calculated by <sup>1</sup>H NMR using CH<sub>3</sub>NO<sub>2</sub> as the internal standard, whereas nonvolatile compounds were purified by flash chromatography.

**2.6. General Procedure for Photocatalytic 6-exo Cyclation.** A vial was charged with a magnetic stirring bar, the halogenated

Scheme 2. PTH Encapsulation Procedure on oSWNT and Synthesis of Hybrids 4 and 5

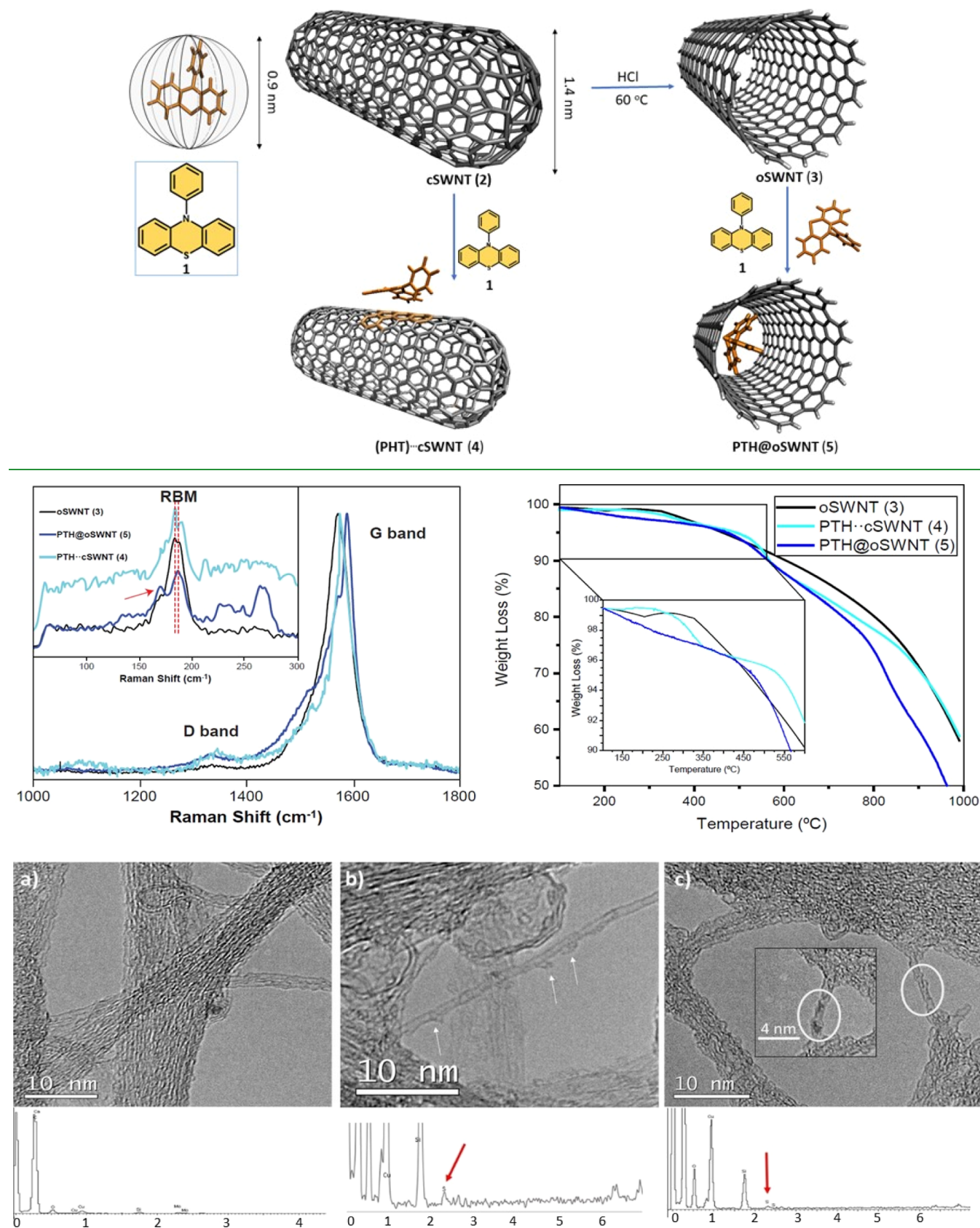


**Figure 1.** Top: Raman spectra of oSWNT (3), (PTH)·cSWNT (4), PTH@oSWNT (5) and their TGA analysis. Bottom: HR-TEM images of (a) oSWNT (3), (b) (PTH)·cSWNT (4) (white arrows highlight PTH molecules outside the SWNT), and (c) PTH@oSWNT (5) samples (inset: magnification, white circles highlight PTH molecules inside the SWNT). Lower panels: EDX spectra (red arrows indicate sulfur content).



substrate **6q** (0.1 mmol), 1 mg of catalyst PTH@oSWNT (**5**), CH<sub>3</sub>CN (1 mL) and diisopropylethylamine (0.1 mmol). The vial was sealed and degassed by three freeze–pump–thaw cycles. The blue LEDs of the reactor were turned on, and the reaction was allowed to proceed at room temperature for the desired time, typically 16 h. Conversions were analyzed by NMR spectroscopy, and yields were calculated after flash chromatography.

**2.7. General Procedure for Photocatalytic  $\alpha$ -Alkylation of Aldehydes.** A vial was charged with a magnetic stirring bar, the halogenated substrate (0.1 mmol), the aldehyde (0.2 mmol), 20 mol % (*S,S*)-2-*tert*-butyl-3,5-dimethylimidazolidin-4-one, 2,6-lutidine (0.36 mmol), DMF (0.5 mL), and 1 mg of catalyst PTH@oSWNT (**5**). The vial was sealed and degassed by three freeze–pump–thaw cycles. The blue LEDs of the reactor were turned on, and the reaction was allowed to proceed at room temperature for the desired time, typically 16 h. Conversions were analyzed by NMR spectroscopy, and yields were calculated after flash chromatography. Enantiomeric excesses were determined by supercritical fluid chromatography.

**2.8. Recycling Experiments.** After the reaction was completed, the nanotube-based photocatalysts were recovered by filtration through PP membranes and then washed for three cycles with acetone and three additional cycles with DCM, sonicating for 5 min between each cycle. After that, the whole filtering membrane with the black cake over was transferred to a beaker, and 5 mL of acetone was added to create a stable suspension that could be safely transferred to the storage vial. Then, the sample was vacuum-dried. After that, the heterogeneous catalysts were submitted to a new catalytic cycle by adding all reagents and the solvent. This procedure was repeated several times. In the case of the homogeneous photocatalyst, endurance tests were performed by adding a fresh reactant mixture to the reaction vessel for several times.

### 3. RESULTS AND DISCUSSION

**3.1. Synthesis and Characterization.** First, we chose PTH (**1**) as a common organic photocatalyst with a widespread application in dehalogenation reactions,<sup>28–30</sup> owning a very high reduction potential appropriate for the hydrodehalogenation of aromatic compounds [ $E^\circ$  (PTH<sup>•+</sup>/PTH<sup>\*</sup>) =  $-2.1$  V versus SCE;  $E^\circ$  (PTH<sup>•+</sup>/PTH) =  $0.68$  V versus SCE; HOMO–LUMO gap for isolated PTH is about 7 eV, (HOMO:  $-6.5$  eV, LUMO:  $0.5$  eV, GAP:  $7$  eV)].<sup>28</sup> To perform the encapsulation of PTH in the inner cavity of the SWNT, we initially calculated the dynamic radius of the molecule, which was found to be  $0.9$  nm according to DFT calculations (see top left, Scheme 2).

Considering that the van der Waals interactions of photocatalyst **1** with the nanotube need about 40% extra volume,<sup>31</sup> we selected from the large variety of different SWNTs those with a  $1.4$  nm diameter capped in their tips [closed SWNT, cSWNT (**2**)] to fulfill the van der Waals PTH volume requirement. Structure **2** was studied by high-resolution transmission electron microscopy (HR-TEM) analysis. It consisted of nanotubes of  $1.4$  nm average diameter and some micrometers in length, which tended to group in bundles of several individual tubes (see Figure S3 in the Supporting Information). In order to encapsulate the PTH, a mild acid treatment in HCl at  $60$  °C for 2 h was performed to open the tips and remove the amorphous carbon and metal particles responsible for the nanotubes' growth. As a result, the tips of the purified oSWNT (**3**) sample were quantitatively opened, and only a few metallic particles were observed after exhaustive HR-TEM observations (see Figure S4 in the Supporting Information for additional images). Once the tips were opened, the encapsulation of the photocatalyst **1** in the inner cavities of oSWNT (**3**) proceeded as shown in Scheme 2.<sup>27,32</sup> A comparison with the encapsulated sample was

performed using a control experiment submitting cSWNT (**2**) to a similar treatment with PTH. However, cSWNT was not treated with HCl, and therefore the tips were closed. Thus, this control experiment pursues decorating the SWNT just on the outer surface, yielding the sample PTH·cSWNT (**4**).

After the synthesis of the different materials, we carried out a panoply of characterizations such as Raman and UV–vis spectroscopies, total internal reflection fluorescence microscopy (TIRFM), HR-TEM, elemental analysis, and thermogravimetric analysis (TGA), combined with time-dependent density functional theory (TD-DFT) calculations, as well as further photocatalytic experiments to ensure the nature of the different samples. Figure 1 displays the Raman spectra of **3**, **4**, and **5** materials. In all cases, the general Raman pattern agrees with the presence of high-purity SWNTs, and all characteristic regions are identified along the spectrum. Indeed, the tangential C–C  $sp^2$  vibrational mode at  $\sim 1580$  cm<sup>−1</sup> (G band) and the radial vibrations of the carbon atoms responsible for the “tube breathing” at  $\sim 200$  cm<sup>−1</sup> (RBM band) came clearly across on the spectra of all samples, whereas only a tiny C- $sp^3$  related vibrational band (D band) can be detected at  $\sim 1340$  cm<sup>−1</sup>. After treating the nanotubes with PTH (**1**) throughout the encapsulation procedure, the  $I_D/I_G$  ratio (carbon nanomaterials standard structure parameter)<sup>33</sup> of PTH@oSWNT (**5**) nicely matched the untreated oSWNT (**3**)  $I_D/I_G$  ratio, passing from  $0.04$  to  $0.07$  (see Table S1 in the Supporting Information). In addition, the G band red shifts  $17$  cm<sup>−1</sup>. These facts indicated that the carbon structure of PTH@oSWNT (**5**) was almost unaltered during the encapsulation treatment and the nanotube became doped in the ground state due to the interaction with the molecule, that is, electronic communication between the nanotube and the PTH is established (see below).<sup>32,33</sup> However, other and more important changes were observed when analyzing the RBM region. After treating oSWNT with **1**, following the encapsulation procedure to yield PTH@oSWNT, a new shoulder at  $168$  cm<sup>−1</sup> appeared, while the position of the main RBM band is red-shifted  $4$  cm<sup>−1</sup> compared with the pristine oSWNT. In addition, new bands appeared at  $270$  cm<sup>−1</sup>. Therefore, the encapsulation treatment seems to locally expand the diameter of the nanotube itself modifying the overall breathing vibrations, which may indicate that the PTH molecule is successfully introduced into the inner cavity and strongly affects the nanotube diameter, which is in agreement with previous reports in the literature.<sup>27,32</sup> A comparison with the PTH·cSWNT sample (**4**) showed an identical  $I_D/I_G$  ratio of  $0.07$ , indicating that the hot treatment was responsible for the increase in  $I_D/I_G$ . Furthermore, no modification was observed in the RBM region of this control sample since the photocatalyst (**1**) did not enter inside the closed nanotube cSWNT (**2**), while the doping effect in the G band shift in this particular sample is not so pronounced as a result of a less efficient electronic communication.<sup>33</sup> The functionalization degree was estimated by TGA (Figure 1 right). A direct comparison of pristine oSWNT and the PTH@oSWNT samples revealed a decomposition step for the encapsulated sample from  $300$  to  $500$  °C, which was not present in the pristine nanotubes. This feature, usually ascribed to the organic molecule decomposition window,<sup>34,35</sup> represents a weight loss of ca. 8%, which is in complete agreement with the N and S contents detected by elemental analysis (see Table S2 in the Supporting Information). Conversely, a more pronounced thermal decomposition was observed for the physisorbed PTH

molecules found on PTH-cSWNT (4) in the same region. This different thermal behavior between the inside and outside functionalized samples confirms the Raman data, indicating that the physisorbed PTH behaves in a different manner compared to the encapsulated molecules present in PTH@oSWNT. Further evidence of the encapsulation can be obtained by direct observation of the samples employing HR-TEM (see bottom, Figure 1). It is important to mention that the oSWNT sample consisted of clean tubular structures because no particles, objects, or protrusions were observed in their inner cavities.

Following the encapsulation treatment with PTH, the structural integrity of the nanotubes was fully preserved in accordance with the Raman data (see bottom-Figure 1). No deformation, rupture, or shortening was observed after the exhaustive analysis. Interestingly, even working at high voltages to obtain the maximum magnification of the instrument, some tubes appeared to be filled with molecular material in a random disposition inside the carbon scaffold (Figure 1c bottom). It would seem that the PTH (1) guests possess Brownian motion induced by the electron beam, or even, they are rapidly decomposing due to beam damage.

The optical properties of the encapsulated sample, PTH@oSWNT, were analyzed by absorption and luminescence UV-vis spectroscopies and compared with those of oSWNT and the photocatalyst PTH (see Figures S9 and S10 in the Supporting Information). Both oSWNT and PTH showed their characteristic absorption bands as previously reported.<sup>30</sup> Indeed, oSWNT presented a strong absorption in the 270 nm region, characteristic of the C–C bonds, and the absorption maximum of the photocatalyst 1 was found at 321 nm. On the other hand, the encapsulated sample PTH@oSWNT presented a maximum red shift at 280 nm, in agreement with the doping effect discussed within the Raman data. The emission spectrum of PTH@oSWNT (5) showed a lower luminescent intensity than that of PTH, indicating the good electron–hole separation efficiency as has been reported for other composite nanotubes.<sup>36</sup> To gain insights into the sample at the nanoscale level, we studied the fluorescence of individual powder microstructures with TIRFM. Using this technique, the evanescent field only excited those aggregates located at less than 100 nm from the focal plane, thus providing a gist of the sample behavior at a nanoscale level. PTH@oSWNT (5) drop-casted from the alcohol suspensions onto glass coverslips was resolved as isolated aggregates. These conglomerated structures sometimes exhibited stripes that are reminiscent of carbon nanotube bundles (Figure 2).<sup>37</sup> It is important to highlight that the fluorescence characterization of oSWNT (3) did not show any contrast in the images.

### 3.2. Photocatalytic Activity, Scope, and Recyclability.

Once the PTH@oSWNT (5) material had been characterized, we evaluated this hybrid material as a photocatalyst. Therefore, we studied the dehalogenation of aromatic compounds<sup>28</sup> under visible-light irradiation as a model reaction, using *p*-bromobenzonitrile (6a) as a starting material (see Table 1). The debromination of 6a was conducted under nitrogen atmosphere with tributylamine as a sacrificial donor and formic acid in CH<sub>3</sub>CN, employing just 1 mg of PTH@oSWNT and obtaining full conversion (loading of PTH = 0.29 mol % according TGA and elemental analysis determinations). To understand the role of each component in our catalytic cycle, different parameters were modified, as depicted in Table 1. First, the reaction required the presence of the catalyst PTH@

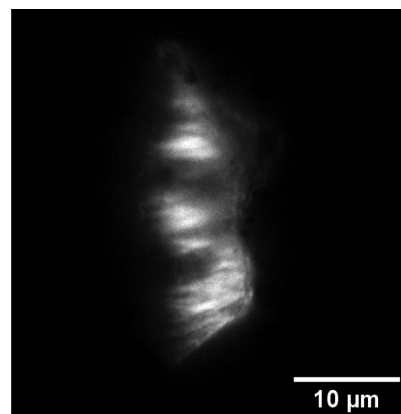


**Figure 2.** Bundled structured of a PTH@oSWNT (5) conglomerate obtained with TIRFM.

**Table 1.** Optimization of *p*-Bromobenzonitrile Debromination Catalyzed by PTH@oSWNT (5)

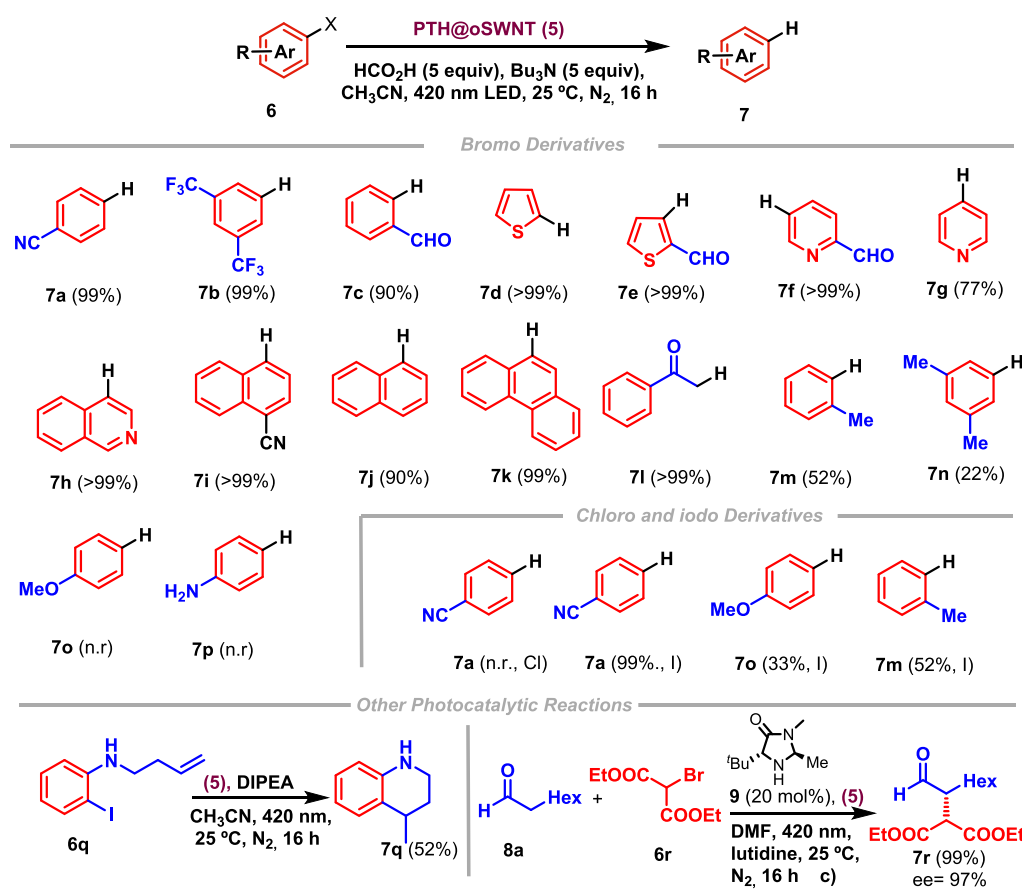
entry <sup>a</sup>	variation from standard conditions <sup>a</sup>	conversion [%] <sup>b</sup>
1	none	>99
2	without 5	18
3	without Bu <sub>3</sub> N	n.r.
4	DIPEA instead Bu <sub>3</sub> N	22
5	no HCO <sub>2</sub> H	n.r.
6	under aerobic conditions	n.r.
7	no light	n.r.
8	[M] = 1.0	93

<sup>a</sup>Reaction conditions: 0.1 mmol of substrate in 1 mL of acetonitrile with 5 equiv Bu<sub>3</sub>N and 5 equiv HCOOH under an inert atmosphere with 1 mg of catalyst for 16 h at r.t. irradiating with 420 nm wavelength. <sup>b</sup>Conversion (%), detected by <sup>1</sup>H NMR; n.r. stands for no reaction.

oSWNT to be successful (entries 1 and 2). The absence of Bu<sub>3</sub>N or its change to DIPEA demonstrated that a sacrificial electron donor was needed for the reaction (entries 3 and 4). In addition, the absence of acid and light or the presence of oxygen resulted in negligible conversions (entries 5–7). Conversely, when the reaction was concentrated to 1 M, a slightly lower conversion was observed (93%) (entry 8). Using these conditions, we tested different halogen derivatives (Table 2). This table shows that the activated electron-poor substrates such as 6b or 6c were successfully debrominated. The use of different heterocyclic rings such as thiophenes (6d and 6e), pyridines (6f and 6g), or isoquinoline (6h) provided the hydrodebrominated products 7d–h in excellent conversions and yields (77–99%). The debromination of the other extended aromatic systems, such as naphthalene or phenanthrene, afforded the compounds 7i–7k. Interestingly, an alkylbromide (6l) can also be employed with a 99% conversion. The presence of electron-donating groups at the aromatic ring provoked a decrease, or even a negligible conversion, due to the high reduction potential of those starting materials (6m–p).

Because the redox potential required to achieve the dehalogenation of aromatic chlorides is very high, catalyst 5

Table 2. Scope of the Dehalogenation Reaction of PTH@oSWNT and Other Photocatalytic Applications



was not able to accomplish this particular reduction under visible light. By contrast, the iodides were easily reduced. The neutral and electron-rich substrates such as iodotoluene and iodoanisole could be reduced employing the catalyst PTH@oSWNT. Interestingly, 5 was able to convert electron-poor substrates such as iodobenzonitrile (7a), which was fully dehalogenated in 16 h. Finally, the catalytic performance of PTH@oSWNT was expanded further by studying different C–C bond formation photoreactions, which are important reactions from a synthetic point of view. Thus, the encapsulated hybrid material was also able to accomplish the light-mediated synthesis of tetrahydroisoquinoline (7q) with a 52% yield, starting from the corresponding iodide 6q in a 6-*exo* cyclization procedure.<sup>38</sup> On the other hand, 5 was able to afford the  $\alpha$ -alkylation of aliphatic aldehydes (8a) with diethyl-bromomalonate 6r with a very good conversion (99%) and enantioselectivity (97% ee).<sup>39,40</sup> To check for any modifications after reaction, the material was also analyzed by Raman spectroscopy, TGA, and elemental analysis, but no alterations were detected (see Figures S7 and S8 in the Supporting Information). In addition, leaching tests were carried out under “hot filtration” conditions. After removing catalyst 5 at 60 and 90% conversions, no further reaction was respectively observed during this time (see Figure S11 in the Supporting Information). These experiments demonstrate that there were not any homogeneous active species in the solution.

Another crucial factor for any heterogeneous catalyst is the ability to be recycled without losing activity (Figure 3). We initially studied the debromination of 6a under the

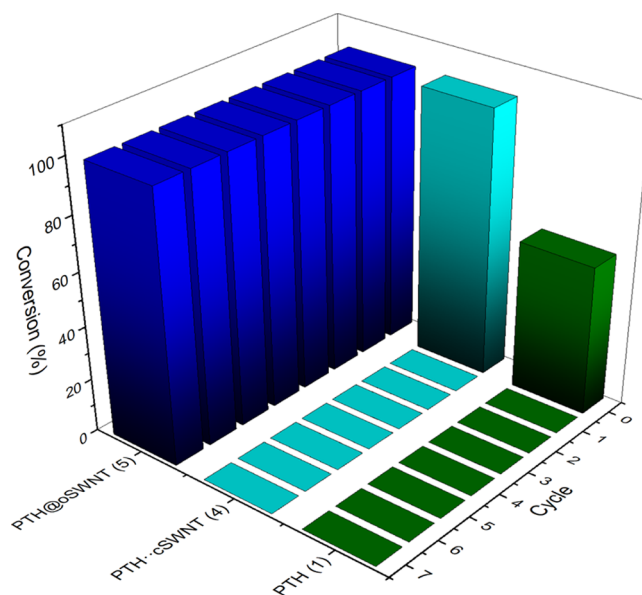
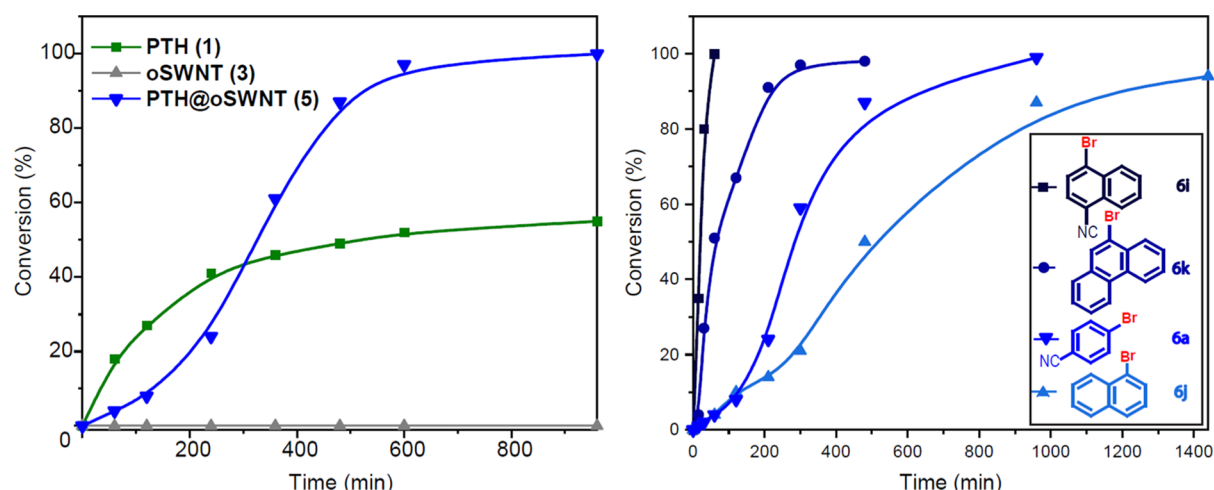


Figure 3. Recycling study of PTH (1), PTH-cSWNT (4), and PTH@oSWNT (5).

homogeneous PTH (1) catalyst (0.29 mol %), obtaining a 56% conversion after 24 h. A fresh batch of reactants added to this reaction media afforded a negligible conversion (dark-green bar), indicating the low stability of the homogeneous photocatalyst 1 under these reaction conditions. The reusability studies of 5 in the debromination were carried





**Figure 4.** Left: kinetic profiles of the *p*-bromobenzonitrile (6a) debromination with different catalysts. 0.29 mol % catalyst was used to mimic the amount of PTH molecules encapsulated in PTH@oSWNT (5) as determined by TGA (*ca.* 8.0% wt). Right: kinetic profiles of the debromination of the condensed aromatics 6i–j, including the model *p*-bromobenzonitrile 6a, catalyzed by 5. The lines are for visual guidance.

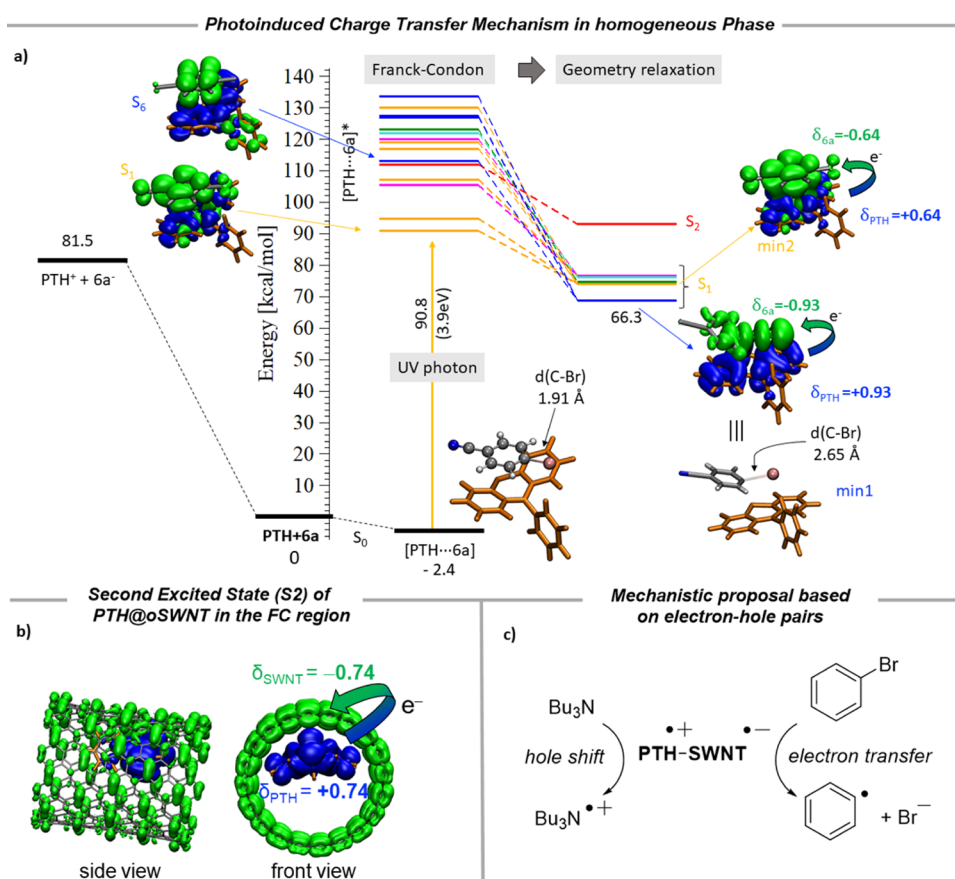


**Figure 5.** (a) Energy profile for the dehalogenation of 6a at the excited state upon light absorption (right side) and at the ground state surface,  $S_0$  (left side). Between them, the energy of the first 15 excited states populated upon UV–vis light absorption by the PTH...6a complex at the FC region is shown. They are colored according to the minima reached after optimization. Insets: excited-ground state electronic density differences for  $S_1$  and  $S_6$  at the FC region and for the minima reached after their optimization (min2 and min1, respectively). The electron density is transferred from the blue region of the molecule toward the green areas upon excitation. (b) Excited-ground state density differences for the second excited state ( $S_2$ ) of the PTH@oSWNT (5) system at the FC region. The electron density moves from the blue region of the molecule toward the green region in the nanotube. (c) Mechanistic proposal starting from the photogenerated PTH<sup>•+</sup>@SWNT<sup>•-</sup> hybrid material.

out by the separation of the catalyst from the reaction mixture, washing and filtering it, and submitting the solid to further cycles by adding fresh reactants (blue bars). After seven cycles, any loss of activity was measured yielding the same conversion

level in all cases. To confirm the stability of 5 after recycling, we analyzed the material by TEM analysis (see Figure S6 in the Supporting Information), identifying PTH molecules inside the nanotubes. This protective environment is even more

outstanding when compared with the supramolecular complex PTH·cSWNT (**4**) (cyan bar). As depicted above, the physisorbed material **4** just owns the PTH molecules on the outer surface of the walls (Figure 1A). Therefore, the  $\pi$ -stacking should provide a similar electronic communication to that of **5** but lacking the protective effect of the encapsulation. Indeed, the same performance (full conversion) for the first cycle was observed using PTH·cSWNT as a photocatalyst in the debromination of **6a**. However, after recovering this black powder and submitting it to the same washing procedure described above, the second cycle resulted in negligible conversion. The same behavior was observed for sample **4'** (see Supporting Information, Figure S11). This was due to the removal of all photoactive molecules during the recovery-washing process as a result of the weak interactions present in this supramolecular structure. Therefore, the nanotubes provide a protective environment, which prevents the photo-degradation of the organic catalyst PTH (**1**) and also makes its recovery and reuse easier.

**3.3. Mechanistic Proposal.** In order to compare the catalytic activity of the homogenous PTH **1** and the new material PTH@oSWNT (**5**), we performed a kinetic profile of the reaction under optimized reaction conditions (left, Figure 4). The control experiment with oSWNT (gray line) showed negligible catalytic activity, whereas the homogeneous catalyst **1** (0.29 mol %) provided a 56% conversion after 16 h following pseudo-first-order kinetics. Regarding PTH@oSWNT, this reaction needed a period of activation (120 min). After this time, material **5** showed outstanding catalytic activity (2-fold) when compared with the homogeneous PTH (green and blue lines). Therefore, this test highlights the enhanced turnover number (TON) that the encapsulated material is able to reach ( $\text{TON}_{\text{PTH@oSWNT}} = 343$  vs  $\text{TON}_{\text{PTH(0.29\%)}} = 189$ , see Table S3 in the Supporting Information), even surpassing the 5.0 mol % catalyst loading typically employed in the literature (see Figure S12 in the Supporting Information). Interestingly, when the reaction was scaled up to 1 mmol, but maintaining the same amount of the material **5**, this TON can even be expanded by 1 order of magnitude ( $\text{TON}_{\text{PTH@oSWNT}} = 3207$ , 1.0 mmol). Thus, PTH@oSWNT (**5**) exhibits a comparable or even better photocatalytic performance compared with other state-of-the-art heterogeneous catalysts previously described by other authors for similar dehalogenation reactions (see Table S4 in the Supporting Information for further details). To understand whether the origin of the induction period was related to the diffusion or absorption of the substrate within the nanotube wall, we performed a series of experiments with different bromoarenes **6i–j** (right, Figure 4). In general, polyaromatic compounds submitted to the photo debromination conditions increased the reaction rate despite the electronic nature of the aromatic ring. Thus, bromo-naphthonitrile (**6i**) was quantitatively debrominated in just 60 min by comparison with *p*-bromobenzonitrile **6a** (900 min), showing that the extended aromaticity (one more phenyl ring in **6i**) favored the  $\pi$ - $\pi$  interactions with the material. The same trend was observed for the nonactivated substrates **6j** and **6k**, where the reaction rate was faster for **6k** (300 vs 1400 min, respectively).

To gain insight into the photocatalytic reaction, we performed quantum chemistry simulations in the frame of the TD-DFT<sup>41–43</sup> (see the Supporting Information for further computational details). We started by studying the photoredox catalytic mechanism with the molecular photocatalyst PTH, using as a model reaction the debromination of **6a**. To this

end, we considered the complex formed by PTH and *p*-bromobenzonitrile (**6a**), named [PTH···**6a**], which was found to be slightly more stable than the two separated moieties by  $-2.4 \text{ kcal mol}^{-1}$  (top-Figure 5). The first 15 excited electronic states of the complex in the Franck–Condon (FC) region lie between 3.9 and 5.8 eV above the ground-state minimum (see a complete characterization of these excitations in Tables S6 and S7 in the Supporting Information). The low-lying excited states are typically associated with  $\pi$ - $\pi^*$  transitions, where the electronic density moves from the  $\pi$  orbitals localized at the phenothiazine core of PTH toward the  $\pi^*$  orbitals at **6a** or toward the  $\pi^*$  orbitals in the perpendicular phenyl ring on PTH. Some of these states showed an important charge transfer character in the FC region, such as  $S_1$  and  $S_6$  in which a positive charge in the PTH moiety of  $\delta_{\text{PTH}} = 0.55$  and  $\delta_{\text{PTH}} = 0.71$ , respectively, was obtained. The evolution of such excited states outside the FC region was explored by optimizing the geometry of the 15 lowest energy excited states. Most of the optimizations converged in stable minima of the  $S_1$  potential energy surface (PES), with only the exception of the fifth excited state, which reached a minimum in the  $S_2$  PES. Interestingly, the most stable minimum in the  $S_1$  PES (**min1**) showed electron density transfer from the  $\pi$  orbital of the phenothiazine core of PTH (blue region) toward a  $\sigma^*$  orbital of **6a** located in the C–Br region (green surface). Indeed, in this minimum, an almost complete charge transfer from PTH toward **6a** ( $\delta_{\text{PTH}} = 0.93$  and  $\delta_{\text{6a}} = -0.93$ ) is accompanied by a strong elongation of the C–Br bond, from the initial 1.91 Å up to 2.65 Å. The second most stable minimum in the  $S_1$  PES (**min2**) showed a similar charge transfer character, in this case, from the PTH  $\pi$  orbitals toward the **6a**  $\pi^*$  orbitals ( $\delta_{\text{PTH}} = 0.64$ ) and without C–Br bond elongation. This minimum will probably evolve toward **min1**. The higher energy minima (**min3–min5**) correspond to the  $\pi$ - $\pi^*$  transitions within the PTH molecule, and therefore, no charge transfer was observed. We stress here that the brightest states evolved toward **min1** or **min2**, that is, an effective charge separation upon UV–vis light irradiation was obtained. Notice that the reduction of **6a** in the electronic ground state is energetically highly demanding, with  $81.5 \text{ kcal mol}^{-1}$  required to obtain the noninteracting compounds with the charge transferred  $\text{6a}^-/\text{PTH}^+$ . Thus, a photoinduced SET catalyzes the reaction. Once the electron has been transferred to **6a**, the C–Br cleavage is much more favorable because the minimum for the anion  $\text{6a}^-$  has a C–Br distance of 2.65 Å, which is 1 Å longer than in the neutral case. Therefore, the SET toward **6a** triggers the debromination reaction by weakening the C–Br bond. Therefore, the photoinduced charge transfer toward the *p*-bromobenzonitrile substrate is the key step in the mechanism. Once the homogeneous photoreduction of **6a** was characterized, we moved to the encapsulated sample PTH@oSWNT (**5**). We computed its first 21 excited states in the FC region (see Tables S9 and S10 in the Supporting Information). In this case, we also found low lying excited states with an important charge transfer character. As an example, the electronic density difference corresponding to second excited state ( $S_2$ ) is shown (Figure 5b). It was clearly observed that the electronic density is transferred from the  $\pi$  system of PTH toward the unoccupied  $\pi$  orbitals at the oSWNT. Comparing this with the debromination mechanism proposed in the homogeneous phase, we could expect those transitions with an important charge transfer character in the FC region to also lead to stable minima in the  $S_1$  PES, where an electron has been transferred



from the PTH molecule to the nanotube. This facilitates the charge separation in the material and enhances the generation of electron–hole pairs at the interface, which are therefore responsible for the catalytic activity of the system. In the next step the electrons injected on the surface of the material can easily be transferred to the bromoarene and trigger the cleavage of the C–Br bond. Finally, the amine ( $\text{Bu}_3\text{N}$ ) acts as a sacrificial hole shifter, with the associated recovery of the catalytic material (Figure 5c).

#### 4. CONCLUSIONS

We have described a convenient and easy strategy for the heterogenization of organic photoredox catalysts, yielding an active material that is able to heterogeneously perform light-mediated SET reactions. The proposed method based on refluxing a solution of PTH in the presence of cap-opened SWNTs was very simple, yielding a hybrid material where 8% of the PTH was encapsulated in the inner cavity of the SWNT, as demonstrated by TEM, Raman, TGA, and elemental analysis. Our material, PTH@oSWNT, was able to perform hydrodehalogenation reactions and more complex transformations such as the synthesis of tetrahydroisoquinolines and  $\alpha$ -alkylation of aldehydes under 420 nm wavelength illumination. The hybrid material PTH@oSWNT enabled an easy recovery employing simple filtration methods, and more than eight catalytic reuses were performed without any evidence of activity loss. The encapsulated PTH was able to transfer the electron generated in the excitation process to the  $\pi$  system of the nanotube. Thus, this electron injection and further electron–hole separation were responsible for the catalytic activity in the visible-light-mediated photoredox SET dehalogenation reactions.

#### ■ ASSOCIATED CONTENT

##### Supporting Information

The Supporting Information is available free of charge at <https://pubs.acs.org/doi/10.1021/acsami.1c04679>.

Synthesis, extended characterization, catalytic data, and computational details (PDF)

#### ■ AUTHOR INFORMATION

##### Corresponding Authors

Matías Blanco – Organic Chemistry Department, Universidad Autónoma de Madrid, 28049 Madrid, Spain;  
Email: [matias.blanco@uam.es](mailto:matias.blanco@uam.es)

José Alemán – Organic Chemistry Department, Universidad Autónoma de Madrid, 28049 Madrid, Spain; Institute for Advanced Research in Chemical Sciences (IAdChem), Universidad Autónoma de Madrid, 28049 Madrid, Spain;  
[orcid.org/0000-0003-0164-1777](https://orcid.org/0000-0003-0164-1777); Email: [jose.aleman@uam.es](mailto:jose.aleman@uam.es)

##### Authors

Daniel González-Muñoz – Organic Chemistry Department, Universidad Autónoma de Madrid, 28049 Madrid, Spain

Ana Martín-Somer – Chemistry Department, Módulo 13, Universidad Autónoma de Madrid, 28049 Madrid, Spain

Klara Strobl – Department of Condensed Matter Physics, Universidad Autónoma de Madrid, 28049 Madrid, Spain

Silvia Cabrera – Inorganic Chemistry Department and Institute for Advanced Research in Chemical Sciences

(IAdChem), Universidad Autónoma de Madrid, 28049 Madrid, Spain; [orcid.org/0000-0002-4907-2932](https://orcid.org/0000-0002-4907-2932)

Pedro J. De Pablo – Department of Condensed Matter Physics and Condensed Matter Physics Center, Universidad Autónoma de Madrid, 28049 Madrid, Spain

Sergio Díaz-Tendero – Chemistry Department, Módulo 13 and Institute for Advanced Research in Chemical Sciences (IAdChem), Universidad Autónoma de Madrid, 28049 Madrid, Spain; [orcid.org/0000-0001-6253-6343](https://orcid.org/0000-0001-6253-6343)

Complete contact information is available at:  
<https://pubs.acs.org/doi/10.1021/acsami.1c04679>

#### Notes

The authors declare no competing financial interest.

#### ■ ACKNOWLEDGMENTS

Financial support was provided by the European Research Council (ERC-CoG, contract number: 647550), the Spanish Government (RTI2018-095038-B-I00, PID2019-110091GB-I00), and the “Comunidad de Madrid” and European Structural Funds (S2018/NMT-4367). M.B. wishes to thank the Spanish Government for a Juan de la Cierva contract (IJC2019-042157-I). A.M.-S. acknowledges support by the Comunidad Autónoma de Madrid under grant 2016-T2/IND-1660. We also acknowledge the generous allocation of computing time at the CCC-UAM and the electron microscopy analysis from CNME. The authors acknowledge Dr. Lara Martínez-Fernández for help and fruitful discussions concerning the excited-state calculations.

#### ■ REFERENCES

- (1) Georgakilas, V.; Perman, J. A.; Tucek, J.; Zboril, R. Broad Family of Carbon Nanoallotropes: Classification, Chemistry, and Applications of Fullerenes, Carbon Dots, Nanotubes, Graphene, Nanodiamonds, and Combined Superstructures. *Chem. Rev.* **2015**, *115*, 4744–4822.
- (2) Lu, J. P. Elastic Properties of Carbon Nanotubes and Nanoropes. *Phys. Rev. Lett.* **1997**, *79*, 1297–1300.
- (3) White, C. T.; Todorov, T. N. Carbon Nanotubes as Long Ballistic Conductors. *Nature* **1998**, *393*, 240–242.
- (4) Zhao, J.; Xie, R.-H. Electronic and Photonic Properties of Doped Carbon Nanotubes. *J. Nanosci. Nanotechnol.* **2003**, *3*, 459–478.
- (5) Schnorr, J. M.; Swager, T. M. Emerging Applications of Carbon Nanotubes. *Chem. Mater.* **2011**, *23*, 646–657.
- (6) Su, D. S.; Perathoner, S.; Centi, G. Nanocarbons for the Development of Advanced Catalysts. *Chem. Rev.* **2013**, *113*, 5782–5816.
- (7) Tasis, D.; Tagmatarchis, N.; Bianco, A.; Prato, M. Chemistry of Carbon Nanotubes. *Chem. Rev.* **2006**, *106*, 1105–1136.
- (8) Karousis, N.; Tagmatarchis, N.; Tasis, D. Current Progress on the Chemical Modification of Carbon Nanotubes. *Chem. Rev.* **2010**, *110*, 5366–5397.
- (9) Georgakilas, V.; Tiwari, J. N.; Kemp, K. C.; Perman, J. A.; Bourlino, A. B.; Kim, K. S.; Zboril, R.; Zboril, R. Noncovalent Functionalization of Graphene and Graphene Oxide for Energy Materials, Biosensing, Catalytic, and Biomedical Applications. *Chem. Rev.* **2016**, *116*, 5464–5519.
- (10) Zhang, Y.; Tang, Z.-R.; Fu, X.; Xu, Y.-J. Engineering the Unique 2D Mat of Graphene to Achieve Graphene-TiO<sub>2</sub> Nanocomposite for Photocatalytic Selective Transformation: What Advantage does Graphene Have over Its Forebear Carbon Nanotube? *ACS Nano* **2011**, *5*, 7426–7435.
- (11) Yang, M.-Q.; Zhang, N.; Xu, Y.-J. Synthesis of Fullerene-, Carbon Nanotube-, and Graphene-TiO<sub>2</sub> Nanocomposite Photo-

catalysts for Selective Oxidation: A Comparative Study. *ACS Appl. Mater. Interfaces* **2013**, *5*, 1156–1164.

(12) Feng, S.-A.; Zhao, J.-H.; Zhu, Z.-P. The Manufacture of Carbon Nanotubes Decorated with ZnS to Enhance the ZnS Photocatalytic Activity. *New Carbon Mater.* **2008**, *23*, 228–234.

(13) Martínez, C.; Canle, L. M.; Fernández, M. I.; Santaballa, J. A.; Faria, J. Kinetics and Mechanism of Aqueous Degradation of Carbamazepine by Heterogeneous Photocatalysis Using Nanocrystalline TiO<sub>2</sub>, ZnO and Multi-walled Carbon Nanotubes–Anatase Composites. *Appl. Catal., B* **2011**, *102*, 563–571.

(14) Narayanam, J. M. R.; Stephenson, C. R. J. Visible Light Photoredox Catalysis: Applications in Organic Synthesis. *Chem. Soc. Rev.* **2011**, *40*, 102–113.

(15) Romero, N. A.; Nicewicz, D. A. Organic Photoredox Catalysis. *Chem. Rev.* **2016**, *116*, 10075–10166.

(16) Skubi, K. L.; Blum, T. R.; Yoon, T. P. Dual Catalysis Strategies in Photochemical Synthesis. *Chem. Rev.* **2016**, *116*, 10035–10074.

(17) Rigotti, T.; Alemán, J. Visible Light Photocatalysis – From Racemic to Asymmetric Activation Strategies. *Chem. Commun.* **2020**, *56*, 11169–11190.

(18) Crespi, S.; Fagnoni, M. Generation of Alkyl Radicals: From the Tyranny of Tin to the Photon Democracy. *Chem. Rev.* **2020**, *120*, 9790–9833.

(19) Strieth-Kalthoff, F.; Glorius, F. Triplet Energy Transfer Photocatalysis: Unlocking the Next Level. *Chem* **2020**, *6*, 1888–1903.

(20) Prier, C. K.; Rankic, D. A.; MacMillan, D. W. C. Visible Light Photoredox Catalysis with Transition Metal Complexes: Applications in Organic Synthesis. *Chem. Rev.* **2013**, *113*, 5322–5363.

(21) Chitta, R.; Sandanayaka, A. S. D.; Schumacher, A. L.; D'Souza, L.; Araki, Y.; Ito, O.; D'Souza, F. Donor-Acceptor Nanohybrids of Zinc Naphthalocyanine or Zinc Porphyrin Noncovalently Linked to Single-Wall Carbon Nanotubes for Photoinduced Electron Transfer. *J. Phys. Chem. C* **2007**, *111*, 6947–6955.

(22) Ogunbayo, T. B.; Nyokong, T. Phototransformation of 4-nitrophenol Using Pd Phthalocyanines Supported on Single Walled Carbon Nanotubes. *J. Mol. Catal. A: Chem.* **2011**, *337*, 68–76.

(23) Ogunbayo, T. B.; Nyokong, T. Photocatalytic Transformation of Chlorophenols Under Homogeneous and Heterogeneous Conditions Using Palladium Octadecylthio Phthalocyanine. *J. Mol. Catal. A: Chem.* **2011**, *350*, 49–55.

(24) Arai, T.; Nobukuni, S.; Sandanayaka, A. S. D.; Ito, O. Zinc Porphyrins Covalently Bound to the Side Walls of Single-Walled Carbon Nanotubes via Flexible Bonds: Photoinduced Electron Transfer in Polar Solvent. *J. Phys. Chem. C* **2009**, *113*, 14493–14499.

(25) Iglesias, D.; Melchionna, M. Enter the Tubes: Carbon Nanotubes Endohedral Catalysis. *Catalysts* **2019**, *9*, 128–147.

(26) de Juan, A.; Pouillon, Y.; Ruiz-González, L.; Torres-Pardo, A.; Casado, S.; Martín, N.; Rubio, Á.; Pérez, E. M. Mechanically Interlocked Single-Wall Carbon Nanotubes. *Angew. Chem., Int. Ed.* **2014**, *53*, 5394.

(27) Jordan, J. W.; Lowe, G. A.; McSweeney, R. L.; Stoppiello, C. T.; Lodge, R. W.; Skowron, S. T.; Biskupek, J.; Rance, G. A.; Kaiser, U.; Walsh, D. A.; Newton, G. N.; Khlobystov, A. N. Host–Guest Hybrid Redox Materials Self-Assembled from Polyoxometalates and Single-Walled Carbon Nanotubes. *Adv. Mater.* **2019**, *31*, 1904182.

(28) (a) Discekici, E. H.; Treat, N. J.; Poelma, S. O.; Mattson, K. M.; Hudson, Z. M.; Luo, Y.; Hawker, C. J.; de Alaniz, J. R. A Highly Reducing Metal-free Photoredox Catalyst: Design and Application in Radical Dehalogenations. *Chem. Commun.* **2015**, *51*, 11705–11708. (b) Pan, X.; Fang, C.; Fantin, M.; Malhotra, N.; So, W. Y.; Peteanu, L. A.; Isse, A. A.; Gennaro, A.; Liu, P.; Matyjaszewski, K. Mechanism of Photoinduced Metal-Free Atom Transfer Radical Polymerization: Experimental and Computational Studies. *J. Am. Chem. Soc.* **2016**, *138*, 2411–2425. (c) Mayer, L.; May, L.; Müller, T. J. J. The Interplay of Conformations and Electronic Properties in N-aryl Phenothiazines. *Org. Chem. Front.* **2020**, *7*, 1206–1217.

(29) Poelma, S. O.; Burnett, G. L.; Discekici, E. H.; Mattson, K. M.; Treat, N. J.; Luo, Y.; Hudson, Z. M.; Shankel, S. L.; Clark, P. G.; Kramer, J. W.; Hawker, C. J.; Read de Alaniz, J. Chemoselective

Radical Dehalogenation and C–C Bond Formation on Aryl Halide Substrates Using Organic Photoredox Catalysts. *J. Org. Chem.* **2016**, *81*, 7155–7160.

(30) Martínez-Gualda, A. M.; Cano, R.; Marzo, L.; Pérez-Ruiz, R.; Luis-Barrera, J.; Más-Ballesté, R.; Fraile, A.; de la Peña O'Shea, V. A.; Alemán, J. Chromoselective Access to Z- or E- Allylated Amines and Heterocycles by a Photocatalytic Allylation Reaction. *Nat. Commun.* **2019**, *10*, 2634.

(31) Britz, D. A.; Khlobystov, A. N. Noncovalent Interactions of Molecules with Single Walled Carbon Nanotubes. *Chem. Soc. Rev.* **2006**, *35*, 637–659.

(32) Nieto-Ortega, B.; Villalva, J.; Vera-Hidalgo, M.; Ruiz-González, L.; Burzurí, E.; Pérez, E. M. Band-Gap Opening in Metallic Single-Walled Carbon Nanotubes by Encapsulation of an Organic Salt. *Angew. Chem., Int. Ed.* **2017**, *56*, 12240–12244.

(33) Dresselhaus, M. S.; Jorio, A.; Hofmann, M.; Dresselhaus, G.; Saito, R. Perspectives on Carbon Nanotubes and Graphene Raman Spectroscopy. *Nano Lett.* **2010**, *10*, 751–758.

(34) Setaro, A.; Adeli, M.; Glaeske, M.; Przyrembel, D.; Bisswanger, T.; Gordeev, G.; Maschietto, F.; Faghani, A.; Paulus, B.; Weinelt, M.; Arenal, R.; Haag, R.; Reich, S. Preserving  $\pi$ -conjugation in Covalently Functionalized Carbon Nanotubes for Optoelectronic Applications. *Nat. Commun.* **2017**, *8*, 14281.

(35) Wang, Y.; Song, X.; Shao, S.; Zhong, H.; Lin, F. An Efficient, Soluble, and Recyclable Multiwalled Carbon Nanotubes-Supported TEMPO for Oxidation of Alcohols. *RSC Adv.* **2012**, *2*, 7693–7698.

(36) Long, R.; Prezhdo, O. V. Asymmetry in the Electron and Hole Transfer at a Polymer–Carbon Nanotube Heterojunction. *Nano Lett.* **2014**, *14*, 3335–3341.

(37) Graugnard, E.; Reifengerger, R.; Walsh, B.; De Pablo, P. J. Electronic Conductance of Multi-Walled Carbon Nanotubes having reliable electrical contacts. *Clusters Nanostruct. Interfaces* **2000**, 123–130.

(38) González-Muñoz, D.; Nova-Fernández, J. L.; Martinelli, A.; Pascual-Coca, G.; Cabrera, S.; Alemán, J. Visible Light Photocatalytic Synthesis of Tetrahydroquinolines Under Batch and Flow Conditions. *Eur. J. Org. Chem.* **2020**, 5995–5999.

(39) Rigotti, T.; Casado-Sánchez, A.; Cabrera, S.; Pérez-Ruiz, R.; Liras, M.; de la Peña O'Shea, V. A.; Alemán, J. A Bifunctional Photoaminocatalyst for the Alkylation of Aldehydes: Design, Analysis and Mechanistic Studies. *ACS Catal.* **2018**, *8*, 5928–5940.

(40) Casado-Sánchez, A.; Uygur, M.; González-Muñoz, D.; Aguilar-Galindo, F.; Nova-Fernández, J. L.; Arranz-Plaza, J.; Díaz-Tendero, S.; Cabrera, S.; Mancheño, O. G.; Alemán, J. 8-Mercaptoquinoline as a Ligand for Enhancing the Photocatalytic Activity of Pt(II) Coordination Complexes: Reactions and Mechanistic Insights. *J. Org. Chem.* **2019**, *84*, 6437–6447.

(41) Adamo, C.; Jacquemin, D. The Calculations of Excited-state Properties with Time-Dependent Density Functional Theory. *Chem. Soc. Rev.* **2013**, *42*, 845–856.

(42) Frisch, M. J. *Gaussian 16*, Revision B.01, can be found under, 2013. <https://gaussian.com/gaussian16/>.

(43) Casida, M. E.; Jamorski, C.; Casida, K. C.; Salahub, D. R. Molecular Excitation Energies to High-lying Bound States From Time-dependent Density-Functional Response Theory: Characterization and Correction of the Time-dependent Local Density Approximation Ionization Threshold. *J. Chem. Phys.* **1998**, *108*, 4439–4449.